A ^{170}Yb Mössbauer spectroscopy and L_{III}-edge study of the Kondo lattice $YbCu_3Al_2$

1996 J. Phys.: Condens. Matter 8 7797

(http://iopscience.iop.org/0953-8984/8/41/023)

J. Phys.: Condens. Matter **8** (1996) 7797–7812. Printed in the UK

A ^{170}Yb Mössbauer spectroscopy and L_{III}-edge study of the Kondo lattice $YbCu_3Al_2$

P Bonville† and E Bauer‡

† CEA, CE Saclay, Département de Recherches sur l'Etat Condensé, les Atomes et les Molécules, 91191 Gif-sur-Yvette, France

‡ Institut für Experimentalphysik, Technische Universität Wien, A-1040 Wien, Austria

Received 22 April 1996, in final form 9 August 1996

Abstract. We present a detailed study of the magnetic and crystal-field properties of the hexagonal Kondo lattice $YbCu_3Al_2$, using ^{170}Yb Mössbauer spectroscopy in the temperature range 0.1 K–50 K. L_{III}-edge x-ray absorption spectra at 10 K and 300 K were also obtained; they indicate that the Yb ion is very close to trivalent over the whole temperature range. In the antiferromagnetic phase, the thermal variation of the Yb^{3+} spontaneous moment has been measured and the derived transition temperature ($T_N = 1.95$ K) is in agreement with previous specific heat and magnetic data. In the paramagnetic phase, the two components g_z and $g_\perp$ of the g-tensor of the Yb^{3+} ground crystal-field doublet have been measured. These g-values cannot be accounted for by a crystal-field-only model, and we interpret this in terms of a Kondo reduction of the paramagnetism ($T > T_N$) and of the spontaneous moment ($T < T_N$), with a Kondo temperature $T_K \simeq 2.3$ K. In addition, the spectra in the antiferromagnetic phase show inhomogeneous broadenings due to the presence of random distortions with respect to the hexagonal Yb site symmetry, and, close to T_N, dynamical effects are clearly evident and allow the Yb^{3+} fluctuation frequency to be measured in the magnetically ordered phase.

1. Introduction

In Ce- or Yb-based intermetallics, hybridization between 4f and conduction band electrons is a common phenomenon [1]. In the strong-hybridization limit, it leads to an intermediate-valence state for the Ce or Yb ion, and in the weak-hybridization limit, to Kondo or heavy-electron properties for the Ce^{3+} or Yb^{3+} ion. One way of varying the strength of the 4f-band electron hybridization is by chemical substitution which can modify the metal density of electronic states at the Fermi energy and push the 4f orbital closer to or further from the Fermi level. Evidence for this effect has been obtained for the Yb-based hexagonal intermetallics $YbCu_{3+x}Al_{2-x}$, with $0 \leqslant x \leqslant 1$ [2, 3]. The thermodynamical and transport properties reported in [2] in this series show that decreasing the Al content increases the hybridization strength: $YbCu_3Al_2$ is a weak Kondo lattice where the crystal-electric-field (CEF) splittings of the Yb^{3+} ion play an important role, and where the Yb^{3+} sublattice orders magnetically below 2 K [4], whereas $YbCu_4Al$ shows a behaviour assignable to a rather high Kondo temperature (a few 10 K) and where no magnetic ordering occurs.

We present here a microscopic study of the magnetic and CEF properties of $YbCu_3Al_2$, in the temperature range 0.1 K–50 K, using ^{170}Yb Mössbauer absorption spectroscopy, and L_{III}-edge x-ray absorption spectra at 10 K and room temperature. The zero-field Mössbauer spectra allowed the characteristics of the magnetic phase (thermal variation of the spontaneous moment and transition temperature) to be accurately determined.

0953-8984/96/417797+16$19.50

Other noticeable features of the low-temperature Mössbauer spectra are: the presence of measurable Yb^{3+} fluctuation frequencies in a small temperature interval on both sides of the magnetic transition, and the influence of random crystal distortions of the Yb site, which could be detected through the particular line broadenings in the magnetically ordered phase. In the paramagnetic phase, a spectrum at $T = 4.2$ K with an applied magnetic field of 4 T allowed the spectroscopic g-tensor of the ground Yb^{3+} Kramers doublet to be measured. Our data show the influence of the Kondo effect on the magnetic properties, and the derived Kondo temperature is in good agreement with a previous estimation. Furthermore, the Mössbauer spectra revealed the presence in our sample of a sizeable spectral contribution (25%) which does not belong to the $YbCu_3Al_2$ main phase, but which is identical to the Mössbauer spectrum obtained in the $YbCu_4Al$ phase. In this work, we shall focus on the study of the $YbCu_3Al_2$ phase. The Mössbauer spectra in compounds with a lower Al content ($YbCu_{3+x}Al_{2-x}$, where x is 0.5, 0.75 and 1) will be the subject of a future publication.

This paper is organized as follows: after a brief description of the crystal structure (section 2) and of the experimental set-up (section 3), the ^{170}Yb Mössbauer absorption spectra in the magnetically ordered phase (section 4) and in the paramagnetic phase (section 5) are reported. In section 6, the Yb^{3+} ground-doublet wavefunction is discussed and the most likely CEF level scheme is derived; this section also contains an analysis of the CEF distortions observed at the Yb site. In section 7 the lineshapes due to electronic fluctuations, observed close to the transition temperature, are analysed. Section 8 contains the L_{III}-edge x-ray absorption spectra and section 9 the discussion of the Kondo properties and the comparison with the neutron diffraction data.

2. Crystal structure

The preparation of the polycrystalline sample is described in [2]. The $YbCu_{3+x}Al_{2-x}$ compounds crystallize into a hexagonal $CaCu_5$-type structure (space group $P6/mmm$). Their crystal structure has been extensively investigated by x-ray and neutron diffraction experiments [2, 4]. In the hexagonal cell of $YbCu_3Al_2$, the Yb atom occupies the (0, 0, 0) position (the 1a site) and is surrounded by six nearest-neighbour Cu atoms in the $z = 0$ plane, located at the vertices of a regular hexagon (2c sites). The next-nearest neighbours are eight Al and four Cu atoms occupying at random the 3g sites in the $z = \pm\frac{1}{2}$ planes, i.e. forming a regular hexagonal prism whose centre is the Yb atom. The point symmetry of the Yb site is thus exactly hexagonal if one considers the nearest neighbours only, and close to hexagonal if one considers both nearest and next-nearest neighbours. As, in a metallic compound, the lattice charges are screened by the conduction electrons, the Cu–Al disorder in the 3g sites should not lead to important distortions of the hexagonal crystal-field potential at the Yb site, and the CEF interaction acting on the Yb^{3+} ion can be considered to be of hexagonal symmetry to a good approximation.

A room temperature x-ray diffractogram of our sample shows the lines of a $CaCu_5$-type structure, with $a = 5.1105(5)$ Å and $c = 4.1371(5)$ Å, and 4% of an unidentified impurity phase. However, as was said in the introduction, the Mössbauer study reveals that our sample is not single phase (besides the 4% impurity). The identification of the extra phase as $YbCu_4Al$ is discussed in subsection 9.2. As the lattice parameters as well as the form factors of Cu and Al in the various $YbCu_{3+x}Al_{2-x}$ phases are very close, these phases cannot be distinguished in the x-ray and neutron diffractograms from the positions and intensities of the lines.

3. Experimental set-up

The Mössbauer transition of the ^{170}Yb isotope ($E_0 = 84.3$ keV) links the ground nuclear state ($I_g = 0$) to the first excited nuclear state ($I = 2$). The spectra were recorded using a neutron-irradiated Tm^*B_{12} γ-ray source mounted on a linear-velocity electromagnetic drive. The linewidth (FWHM) of the source versus a reference $YbAl_3$ absorber is 2.8 mm s^{-1} (1 mm s^{-1} = 68 MHz for ^{170}Yb). The spectra below 4.2 K were recorded in a ^{3}He–^{4}He dilution refrigerator; temperatures above 1 K can easily be obtained by setting a thermal impedance between the dilution chamber and the sample holder. The spectrum with a magnetic field was recorded using a superconducting coil where the field direction can be set either parallel or perpendicular to the γ-ray propagation direction.

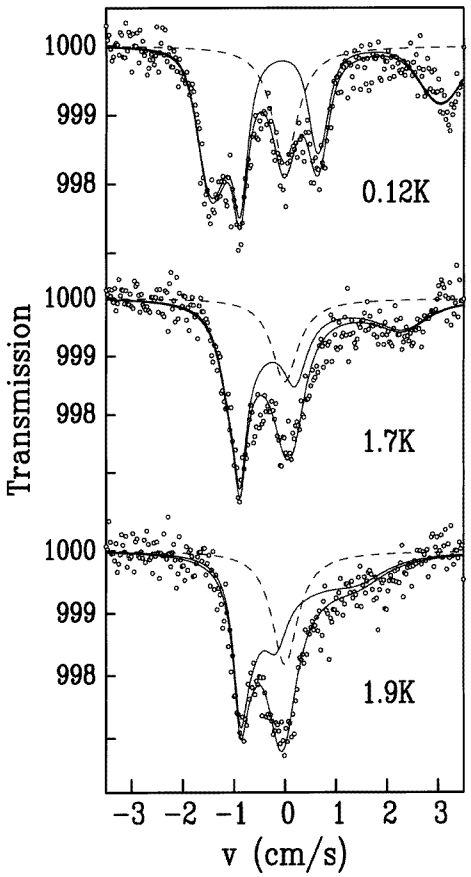

Figure 1. ^{170}Yb Mössbauer absorption spectra in our $YbCu_3Al_2$ sample at selected temperatures in the magnetically ordered phase. The dashed line (Lorentzian line) represents the extra phase contribution, probably from $YbCu_4Al$. The thin solid line represents the $YbCu_3Al_2$ phase spectrum: at $T = 0.12$ K, it corresponds to a fit with correlated distributions of hyperfine fields and quadrupolar parameters; at $T = 1.7$ and 1.9 K, it corresponds to a fit with a relaxational lineshape, as explained in section 7.

The XANES (x-ray absorption near-edge structure) experiments were performed at the French Synchrotron Radiation Facility (LURE) in Orsay using the x-ray beam of the DCI

storage ring (working at 1.85 GeV and ∼220 mA) on the EXAFS D21 station. A double Si(311) crystal was used as a monochromator. Experiments were carried out in a standard manner [5], at 300 K and 10 K, in the energy range 8940 eV to 9020 eV, which contains the L_{III} edge of Yb. Finely powdered samples were spread on an adhesive Kapton tape and four such tapes were stacked together to obtain a sufficiently large signal. This was also helpful in eliminating, to a good extent, any out-of-sample regions in the path of the radiation.

4. ^{170}Yb Mössbauer spectra in the magnetically ordered phase ($T < 2$ K)

4.1. The spectrum at $T = 0.12$ K

The spectrum at $T = 0.12$ K shows a resolved hyperfine structure (figure 1), which consists of two spectral contributions.

The majority contribution (≃75%; the thin solid line in figure 1) corresponds to the sum of a magnetic and of an axially symmetric quadrupolar hyperfine interactions described by the Hamiltonian

$$\mathcal{H}_{hf} = -g_n\mu_n I_z H_{hf} + \frac{eQV_{zz}}{8}\left[I_z^2 - \frac{I(I+1)}{3}\right]. \qquad (1)$$

In this expression, $g_n\mu_n \boldsymbol{I}$ and Q are respectively the magnetic and quadrupolar moment of the excited nuclear state ($I = 2$); Oz is the principal axis of the electric-field-gradient (EFG) tensor at the nucleus site, and $\boldsymbol{H}_{hf}$ and V_{zz} are respectively the hyperfine field, assumed to be directed along Oz, and the main component of the EFG tensor. The majority spectrum is well fitted using this axially symmetric Hamiltonian (the asymmetry parameter η of the EFG tensor is lower than 0.1), which shows that the hyperfine field is directed along the z-axis. This principal axis is a symmetry axis for the EFG tensor and therefore can be identified as the crystal hexagonal $\boldsymbol{c}$-axis. The fitted values at $T = 0.12$ K are $H_{hf} = 290(10)$ T and $\alpha_Q = eQV_{zz}/8 = 4.45(5)$ mm s^{-1}. Such a spectrum is characteristic of an array of magnetically ordered Yb^{3+} ions, located at an axially symmetric site. For rare earths, the spontaneous electronic moment $\boldsymbol{m}$ is proportional to the hyperfine field: $\boldsymbol{m} = \boldsymbol{H}_{hf}/C$, where C is 102 T/μ_B for $^{170}Yb^{3+}$. The ordered Yb^{3+} moments are therefore parallel to the $\boldsymbol{c}$-axis and their amplitude at $T = 0.12$ K (saturated value) is $m(0\ \text{K}) = 2.84(10)\ \mu_B$. Assigning to the ground Kramers doublet an effective spin $S = 1/2$, the z-component of its g-tensor is therefore $g_z = 2m(0\ \text{K})/\mu_B = 5.68(20)$. This majority spectral component corresponds to the $YbCu_3Al_2$ phase, which has been shown, by neutron diffraction experiments [4], to order antiferromagnetically with magnetic moments along the $\boldsymbol{c}$-axis.

The minority spectral component (≃25%; the dashed line in figure 1), consists of a single line (FWHM ≃ 6.2 mm s^{-1}) centred near zero relative velocity. As discussed in section 8, our preliminary ^{170}Yb Mössbauer study of $YbCu_4Al$ strongly suggests that this spectral component corresponds to this latter compound.

4.2. Thermal variation of the spectrum in the ordered phase

The spectra can be satisfactorily fitted to the hyperfine Hamiltonian (1) up to 1.5 K: the hyperfine field $H_{hf}(T)$ steadily decreases as temperature increases, reaching a value of 230 T at 1.5 K, and the quadrupolar coupling parameter α_Q remains at its saturated value 4.45 mm s^{-1}. In this temperature range (0.12 K–1.5 K), the spectra show inhomogeneous line broadenings which can be attributed to the random distortions of the Yb site due to

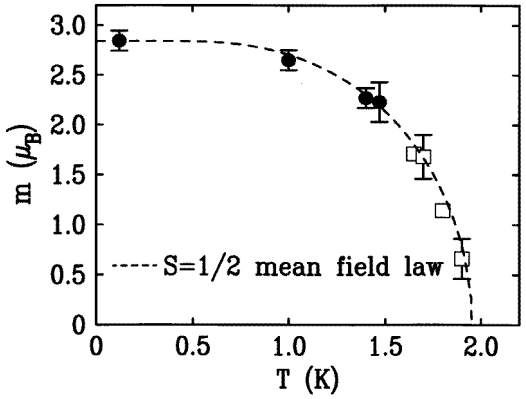

Figure 2. Thermal variation of the Yb^{3+} spontaneous moment in $YbCu_3Al_2$. The solid circles correspond to the hyperfine-field-derived values, and the open squares to the values derived from the exchange-splitting values fitted with the relaxational lineshape (see section 7).

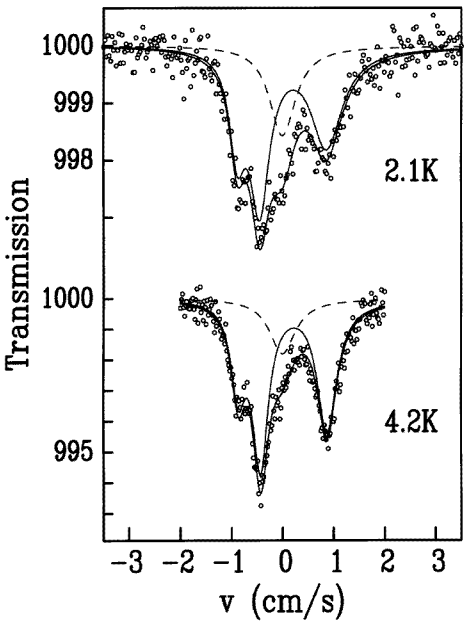

Figure 3. ^{170}Yb Mössbauer absorption spectra for our $YbCu_3Al_2$ sample at selected temperatures in the paramagnetic phase. The dashed line (Lorentzian line) represents the extra phase contribution, probably from $YbCu_4Al$. The thin solid lines represent the $YbCu_3Al_2$ phase spectrum, fitted with a relaxational lineshape (see section 7).

crystal defects. An analysis of these effects in terms of a crystal-field model is performed in subsection 6.2. In the temperature range 1.5–2 K, strong spectral changes are observed, which are not merely increased line broadenings, but which involve changes of the lineshape: the magnetic hyperfine structure is progressively smeared out and the most energetic line drastically broadens (see the 1.9 K spectrum in figure 1). These effects are clearly of

dynamic origin, arising from the fluctuations of the Yb^{3+} ion. They overcome the static broadenings and have to be analysed separately. We shall postpone the analysis of these relaxation effects, which cannot be accounted for by Hamiltonian (1) alone, to section 7. The thermal variation of the spontaneous Yb^{3+} moment is represented in figure 2. The hyperfine-field-derived values ($T \leqslant 1.5$ K; the full circles in figure 2) and the moment values obtained from the relaxation lineshape analysis (1.5 K $< T <$ 2 K; the open squares in figure 2) fit together well and their thermal variation follows a mean-field $S = \frac{1}{2}$ law with $T_N = 1.95$ K, expected for a ground Yb^{3+} Kramers doublet. The magnetic transition is thus second order in $YbCu_3Al_2$, and the derived T_N-value is in good agreement with those obtained from specific heat and magnetic susceptibility data [2].

At a given temperature T, the spontaneous moment $m(T)$, the exchange field $\boldsymbol{H}_{ex}$, directed along the crystal $\boldsymbol{c}$-axis, and the exchange splitting Δ_{ex} are linked by the relations

$$\begin{aligned} \Delta_{ex}(T) &= g_z \mu_B H_{ex}(T) \\ m(T) &= \frac{1}{2} g_z \mu_B \tanh \frac{\Delta_{ex}}{2k_B T}. \end{aligned} \tag{2}$$

One can obtain an estimation of the saturated value of Δ_{ex}, and hence of the saturated H_{ex}-value, using the moment value at 1 K: $m(1\text{ K}) = 2.65\ \mu_B$, which is close to saturation. Using (2), one gets $\Delta_{ex}(1\text{ K}) = 3.3$ K and $H_{ex}(1\text{ K}) \simeq 0.9$ T. Assuming $H_{ex}(0\text{ K}) = 1$ T, we obtain the antiferromagnetic molecular-field constant along $\boldsymbol{c}$: $\lambda_c = H_{ex}(0\text{ K})/m(0\text{ K}) = -0.35\text{ T}/\mu_B$. The saturated value of Δ_{ex} is then $\Delta_{ex}(0\text{ K}) = 3.8$ K, very close to the value $2T_N$ predicted by molecular-field theory.

5. ^{170}Yb Mössbauer spectra in the paramagnetic phase

5.1. Zero-field spectra

In the temperature range 2 K $\leqslant T \leqslant$ 2.2 K, the spectra still provide evidence for the influence of Yb^{3+} paramagnetic fluctuations (figure 3), whose analysis will be presented in section 7. Above 2.3 K, the spectra correspond to an axially symmetric hyperfine quadrupolar interaction in the fast-relaxation regime and can be fitted to the Hamiltonian

$$\mathcal{H}_Q = \{\alpha_Q^{latt} + \alpha_Q^{4f}(T)\}\left[I_z^2 - \frac{I(I+1)}{3}\right]. \tag{3}$$

The two contributions to the quadrupolar coupling parameter are:

(i) a temperature-independent term α_Q^{latt} due to the EFG created by the lattice charges at the nucleus site;

(ii) a term due to the distortion of the 4f shell in a non-cubic CEF, which bears all the temperature dependence and which is proportional to the thermal average of the z-component of the 4f-shell EFG tensor $V_{zz}(T)$, or equivalently, as we express it here, to the z-component of the 4f quadrupolar moment $Q_{zz}(T)$:

$$\alpha_Q^{4f}(T) = B_Q Q_{zz}(T) = B_Q \sum_i \frac{1}{\mathcal{Z}} \mathrm{e}^{-\Delta_i/k_B T} \langle i|3J_z^2 - J(J+1)|i\rangle. \tag{4}$$

In this expression, $\boldsymbol{J}$ is the total angular momentum of the ground spin–orbit multiplet of the Yb^{3+} ion ($J = 7/2$), the states $|i\rangle$ are the eigenstates of the hexagonal CEF interaction with energies Δ_i, $\mathcal{Z}$ being the partition function, and B_Q is a quadrupolar hyperfine constant which is $B_Q \simeq 0.276$ mm s^{-1} for $^{170}Yb^{3+}$.

The experimental thermal variation of $\alpha_Q(T) = \alpha_Q^{latt} + \alpha_Q^{4f}(T)$ is weak: it decreases from 4.35(15) mm s^{-1} at 3 K to 3.85(25) mm s^{-1} at 50 K. This indicates that the energy of the first excited CEF state is of magnitude ∼100 K, and that its quadrupolar moment (or α_Q-value) has the same positive sign as the ground doublet (see also subsection 6.1).

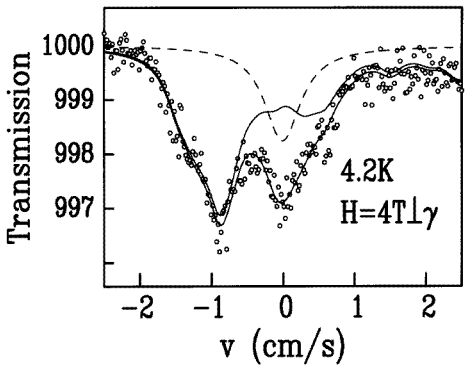

Figure 4. The ^{170}Yb Mössbauer absorption spectrum for our $YbCu_3Al_2$ sample at 4.2 K with a magnetic field of 4 T applied perpendicular to the γ-ray direction of propagation. The dashed line (Lorentzian line) represents the extra phase contribution, probably from $YbCu_4Al$, and the thin solid line the $YbCu_3Al_2$ phase spectrum, fitted as explained in subsection 5.2.

5.2. The spectrum at $T = 4.2$ K with a magnetic field of 4 T

In a polycrystalline sample where the Yb^{3+} ion lies at a site with axial symmetry (the crystal $\boldsymbol{c}$-axis in $YbCu_3Al_2$), application of a magnetic field in the paramagnetic phase allows the two components g_z and $g_\perp$ of the ground-doublet g-tensor to be measured [6], provided that the crystallites do not rotate under the influence of the field. Indeed, for a given crystallite where the $\boldsymbol{c}$-axis is at an angle θ to the applied field, the magnetic moment direction and magnitude (and hence those of the hyperfine field) are completely determined by the g_z- and $g_\perp$-values. The hyperfine energies and line amplitudes depend then on g_z, $g_\perp$ and θ, and the spectrum due to one crystallite can be computed. The Mössbauer powder spectrum is then obtained by integration over space, assuming a random orientation of the crystallites, i.e. of the local $\boldsymbol{c}$-axis, with respect to the field. The shape of this powder spectrum is very sensitive to g_z and $g_\perp$ and allows a rather precise determination of their values. In the spectrum calculation, we did not include the effects of the exchange interaction which, at 4.2 K, is expected to yield only small corrections.

The spectrum obtained at 4.2 K in our powder $YbCu_3Al_2$ sample, where the grains are glued with a G.E. varnish, with a field of 4 T applied perpendicularly to the γ-ray direction of propagation, is shown in figure 4. The single-line component (the dashed line in figure 4) is observed with the same characteristics as in the zero-field spectra. The fit of the $YbCu_3Al_2$ component yields the following values for the g-tensor: g_z = 5.71(13) and $g_\perp/g_z \leqslant 0.25$. The g_z-value obtained is in excellent agreement with that derived from the saturated moment value (5.68; see section 4.1).

In order to get a more precise determination of the $g_\perp$-value, we compared the magnetization curve at $T = 1.5$ K, in the antiferromagnetic phase, obtained for polycrystalline $YbCu_3Al_2$ [2] with a calculated curve. The powder magnetization calculation is similar to that of the Mössbauer spectrum; it involves the g_z- and $g_\perp$-values, and includes

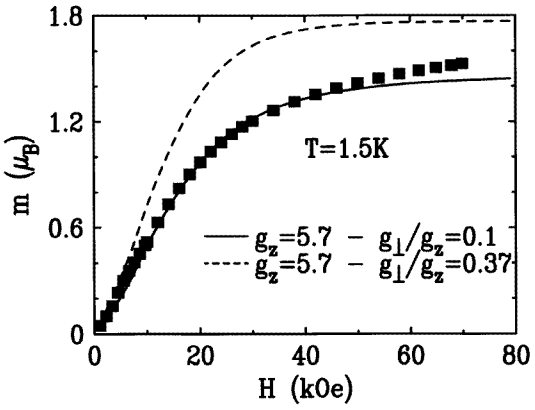

Figure 5. The magnetization curve at $T = 1.5$ K for a polycrystalline $YbCu_3Al_2$ sample (squares), taken from reference [2]. The lines are theoretical curves, calculated with the g-tensor values shown in the figure, and with an isotropic molecular-field constant $\lambda = -0.35$ T/μ_B. Dashed line: the g-tensor as deduced from the values of g_z and $\alpha_Q(T = 0)$ within a hexagonal crystal-field model; solid line: the effective g-tensor deduced from experiment.

the antiferromagnetic exchange interaction, assumed to be isotropic and treated in a self-consistent way. We find that the magnetization data at $T = 1.5$ K are well reproduced, using the previously derived values $g_z = 5.7$ and $\lambda_c = -0.35$ T/μ_B, with a ratio $g_\perp/g_z \simeq 0.1$ (figure 5, solid line). The quasi-saturated high-field value of the powder magnetization is quite sensitive to the $g_\perp$-value, as can be seen in figure 5, where the dashed line represents the $m(H)$-curve with $g_\perp/g_z = 0.37$ (see section 6). The small discrepancy between theory and experiment at high fields arises from the fact that the quantum mixing with the excited states was not taken into account in the calculation.

Table 1. Values of the z-components g_z, Q_{zz}, and of α_Q for the eigenstates $|J = 7/2; J_z = \pm m_s\rangle$ of J_z . The Landé factor is $g_J = 8/7$ for Yb^{3+}.

m_s	$\pm 1/2$	$\pm 3/2$	$\pm 5/2$	$\pm 7/2$
g_z	1.14 ($=g_J$)	3.43 ($=3g_J$)	5.71 ($=5g_J$)	8 ($=7g_J$)
Q_{zz}	−15	−9	3	21
α_Q (mm s^{-1})	−4.140	−2.484	0.828	5.800

6. The Yb^{3+} CEF energies and wavefunctions in $YbCu_3Al_2$

In a crystal-field potential with hexagonal symmetry, the ground spin–orbit multiplet $\{J = 7/2\}$ of the Yb^{3+} ion is split into four Kramers doublets, which are the eigenfunctions of the hexagonal CEF Hamiltonian [7]:

$$\mathcal{H}_{hex} = B_2^0 O_2^0 + B_4^0 O_4^0 + B_6^0 O_6^0 + B_6^6 O_6^6 \tag{5}$$

where the B_n^m are tabulated numerical coefficients and the O_n^m are crystal-field equivalent operators within the $\{J = 7/2\}$ multiplet. The eigenstates of this Hamiltonian are readily

found; using the notation $|m\rangle = |J = 7/2;\ J_z = m\rangle$, they are

$$\begin{aligned} |\psi_1\rangle &= \alpha|\pm\tfrac{7}{2}\rangle + \beta|\mp\tfrac{5}{2}\rangle \\ |\psi_2\rangle &= \beta|\mp\tfrac{7}{2}\rangle - \alpha|\pm\tfrac{5}{2}\rangle \\ |\psi_3\rangle &= |\pm\tfrac{1}{2}\rangle \\ |\psi_4\rangle &= |\pm\tfrac{3}{2}\rangle. \end{aligned} \tag{6}$$

Using the measured values of the ground-doublet g-tensor and of $\alpha_Q(0\ \mathrm{K})$, one can try to derive the ground Yb^{3+} wavefunction; using the thermal variation of $\alpha_Q(T)$, one can get an estimation of the CEF level scheme of the Yb^{3+} ion. In this section, we shall also analyse the inhomogeneous line broadenings of the $T = 0.12$ K spectrum in terms of axial distortions from the exact symmetry of the Yb site.

6.1. The ground-doublet wavefunction and CEF level scheme

From the values $g_z \simeq 5.7$ and $\alpha_Q(0\ \mathrm{K}) \simeq 4.45$ mm s^{-1}, inspection of table 1 shows that the ground wavefunction contains a dominant $|\pm\frac{7}{2}\rangle$ contribution. The following wavefunction:

$$|\psi_1\rangle = 0.912|\pm\tfrac{7}{2}\rangle \pm 0.410|\mp\tfrac{5}{2}\rangle \tag{7}$$

yields the correct value for g_z, and $\alpha_Q^{4f}(0\ \mathrm{K}) = 5$ mm s^{-1}. Keeping in mind that the lattice contribution to the EFG is much smaller than the 4f contribution, and that it can be of opposite sign, agreement with the experimental α_Q-value is obtained with $\alpha_Q^{latt} \simeq -0.6$ mm s^{-1}. However, the wavefunction (7) yields a ratio $g_\perp/g_z$ of 0.40, which is much higher than the experimental value: $g_\perp/g_z = 0.1$, and is compatible neither with the Mössbauer spectrum at $T = 4.2$ K with a field of 4 T nor with the magnetization curve at $T = 1.5$ K (the dashed line in figure 5). Actually, the experimentally derived g-tensor ($g_z = 5.7$, $g_\perp/g_z = 0.1$) does not correspond to any of the expected hexagonal CEF wavefunctions (6). This discrepancy will be further discussed in subsection 9.1 and interpreted in terms of the Kondo coupling on the Yb^{3+} ion.

The weak thermal variation of $\alpha_Q(T)$ up to 50 K implies that the $|\pm\frac{1}{2}\rangle$ and $|\pm\frac{3}{2}\rangle$ states, which have negative values of the quadrupolar moment (see table 1), lie at an energy more than 150 K from the ground state. The most likely situation is that the state $|\psi_2\rangle$, orthogonal to $|\psi_1\rangle$, is the first excited state, with an energy greater than 80 K in order to reproduce the thermal variation $\alpha_Q(T)$.

6.2. Crystal-field distortions and line broadenings in the magnetically ordered phase

The random crystal distortions present in any sample can lead to non-negligible spectral effects, because the ground wavefunctions at each Yb site are modified by mixing with excited states through the distortion (or strain) interaction. In the magnetically ordered phase, strain mixing has been shown to have a measurable influence on the hyperfine spectrum [8]: the spectral lines acquire different (or inhomogeneous) broadenings due to correlated distributions of hyperfine fields and EFG values induced by the strain distribution. In the case where the distortion interaction can be treated as a perturbation with respect to the CEF splittings, this correlation is merely a linear relationship between the hyperfine field and the EFG values (or α_Q-values), independent of the strain variable:

$$\alpha_Q = AH_{hf} + D \tag{8}$$

where A and D are parameters which depend on the wavefunctions of the states involved in the mixing, and on the distortion type. The $YbCu_3Al_2$ spectrum at $T = 0.12$ K

shows inhomogeneous line broadenings and can be very satisfactorily fitted to a gaussian distribution of H_{hf}-values, with a linearly correlated distribution of α_Q-values according to (8) (the thin solid lines in figure 1). The fitted A- and D-values are $A = 0.7(1) \times 10^{-2}$ mm s^{-1} T^{-1} and $D = 2.40(10)$ mm s^{-1}, and the root m.s.d. of the field distribution is $\sigma(H_{hf}) = 37(5)$ T. In order to interpret this finding, we choose a model with the simplest possible axial distortion interaction:

$$\mathcal{H}_{dis} = \epsilon O_2^0 = \epsilon[3J_z^2 - J(J+1)]. \tag{9}$$

This distortion Hamiltonian superposes on Hamiltonian (5) to determine the wavefunctions of the Yb^{3+} ion. The variable ϵ in Hamiltonian (9) can be considered as a deviation of the B_0^2-parameter from an average value, and it is assumed to be distributed according to a symmetrical gaussian law, with root m.s.d. $\sigma(\epsilon)$. Such a distortion can only mix the ground state $|\psi_1\rangle$ with the excited state $|\psi_2\rangle$, at an energy Δ. Using the fact that the matrix elements of J_z and J_z^2 connecting $|\psi_1\rangle$ and $|\psi_2\rangle$ are both equal to $6\alpha\beta$, a simple first-order perturbation calculation yields the perturbed ground wavefunction and the perturbed ground magnetic and quadrupolar moments for a given value of ϵ:

$$\begin{aligned} |\psi_1'\rangle &= |\psi_1\rangle - 18\alpha\beta\frac{\epsilon}{\Delta}|\psi_2\rangle \\ m &= -g_J\mu_B\langle\psi_1'|J_z|\psi_1'\rangle = m_0 + \frac{216\alpha^2\beta^2\epsilon}{\Delta}g_J\mu_B \\ Q_{zz} &= \langle\psi_1'|3J_z^2 - J(J+1)|\psi_1'\rangle = Q_{zz}^0 + \frac{648\alpha^2\beta^2\epsilon}{\Delta} \end{aligned} \tag{10}$$

where $m_0 = \frac{1}{2}g_z\mu_B$ and Q_{zz}^0 are the unperturbed moment values. From these relations, the linear correlation coefficients between the hyperfine field $H_{hf} = Cm$ and the quadrupolar coupling parameter $\alpha_Q = B_Q Q_{zz}$ are easily derived:

$$A = \frac{3B_Q}{g_J}\frac{1}{C\mu_B} \qquad \text{and} \qquad D = B_Q\left(Q_{zz}^0 - \frac{3}{g_J}\frac{m_0}{\mu_B}\right). \tag{11}$$

The slope A does not depend on the α- and β-values and is $A = 0.71 \times 10^{-2}$ mm s^{-1} T^{-1}, in excellent agreement with the experimental value $0.70(10) \times 10^{-2}$ mm s^{-1} T^{-1}. Using $B_Q Q_{zz}^0 = \alpha_Q = 4.45$ mm s^{-1} and $m_0/\mu_B = 2.84$, one gets $D = 2.39$ mm s^{-1}, also in excellent agreement with experiment. The root m.s.d of the hyperfine-field distribution $\sigma(H_{hf})$ is linked to the root m.s.d. of the distortion distribution $\sigma(\epsilon)$ by

$$\sigma(H_{hf}) = 216\alpha^2\beta^2 g_J C\mu_B\frac{\sigma(\epsilon)}{\Delta}. \tag{12}$$

Using the fitted value $\sigma(H_{hf}) = 37$ T, one gets $\sigma(\epsilon)/\Delta \simeq 10^{-2}$, with $\alpha = 0.91$ as in the wavefunction (7). As the CEF splitting Δ is of the order of magnitude of 100 K, we obtain $\sigma(\epsilon) \simeq 1$ K. This is a correct order of magnitude for random strains due to lattice imperfections or defects. The root m.s.d. of this strain distribution is not small with respect to T_N (2 K), and this can contribute to a small distribution of T_N-values, leading to a broadening of the specific heat anomaly at T_N.

7. The Yb^{3+} fluctuations close to the magnetic transition

The spectra of $YbCu_3Al_2$ in the ordered phase at 1.7 K and 1.9 K (the thin solid line in figure 1) and in the paramagnetic phase at 2.1 K (the thin solid line in figure 3) show lineshapes characteristic of the presence of electronic fluctuations with a frequency ν within

the Mössbauer 'relaxation window' for the ^{170}Yb isotope, i.e. $\nu \sim \Delta E_{hf} \sim 1$ GHz, where ΔE_{hf} is the hyperfine line separation. Practically, this frequency window ranges from 50 MHz to 50 GHz, and the spectra around 2 K in $YbCu_3Al_2$ are in the quasi-rapid-relaxation regime, where the magnetic hyperfine structure is almost entirely smeared out and $\nu \sim 10$ GHz.

In the paramagnetic phase, for an axially symmetric Kramers doublet, an analytic perturbative relaxation lineshape has been derived [9] which depends on two dynamic parameters, W_z and $W_\perp$. The electronic fluctuations are assumed to be due to the coupling of the electronic moment to a fluctuating effective magnetic field $\boldsymbol{H}(t)$. For a Kramers doublet, we can write the relaxation interaction as a function of its effective spin $\boldsymbol{S}(S = 1/2)$:

$$\mathcal{H}_{rel} = S_z H_z(t) + \frac{1}{2}[S_+ H_-(t) + S_- H_+(t)]. \tag{13}$$

The W_z- and $W_\perp$-parameters are the Fourier transforms, at zero energy, respectively, of the autocorrelation function $H_z(t)$ and of the correlation function of $H_+(t)$ and $H_-(t)$. The spectra above 2 K were fitted with this lineshape.

We have extended this lineshape to the case of the magnetically ordered phase by taking into account the exchange splitting Δ_{ex} of the ground Kramers doublet. The relaxation parameters are now W_z and the 'up' and 'down' relaxation rates between the exchange-split states of the doublet, $W_\perp^\uparrow$ and $W_\perp^\downarrow$:

$$\begin{aligned} W_\perp^\uparrow &= \frac{1}{\hbar^2}\int_{-\infty}^{+\infty} \mathrm{d}\tau \ \exp\left(-\mathrm{i}\frac{\Delta_{ex}}{\hbar}t\right)\langle H_+(0)H_-(\tau)\rangle \\ W_\perp^\downarrow &= \frac{1}{\hbar^2}\int_{-\infty}^{+\infty} \mathrm{d}\tau \ \exp\left(\mathrm{i}\frac{\Delta_{ex}}{\hbar}t\right)\langle H_-(0)H_+(\tau)\rangle. \end{aligned} \tag{14}$$

The two transverse relaxation rates obey the detailed-balance relation:

$$W_\perp^\uparrow / W_\perp^\downarrow = \exp(-\Delta_{ex}/k_B T)$$

and are related to the usual longitudinal relaxation time T_1 by

$$\frac{1}{T_1} = W_\perp^\uparrow + W_\perp^\downarrow. \tag{15}$$

The lineshape parameters are then $1/T_1$, W_z and Δ_{ex}. The spectra between 1.5 K and 1.9 K were fitted with this lineshape, the g-tensor being fixed at the previously measured values: $g_z = 5.7$ and $g_\perp/g_z = 0.1$.

The fits are very satisfactory both below and above T_N. For $T < T_N$, the fitted values of Δ_{ex} yield the moment values, according to (2); for instance, at $T = 1.7$ K, we obtain $\Delta_{ex} = 2.3(4)$ K and $m = 1.7(2)\ \mu_B$. The spontaneous-moment values obtained this way are reported in figure 2 as open squares, and match well with the hyperfine-field-derived values. As to the dynamic parameters, it transpires that the lineshapes are almost independent of the longitudinal parameter W_z; thus we could only measure $1/T_1$, given by (15) below T_N, and by $1/T_1 = 2W_\perp$ above T_N. Below T_N, we find that $1/T_1 = 5.0(1.5)$ GHz is temperature independent, the change in the lineshape being due to the thermal variation of Δ_{ex} alone. Above T_N, $1/T_1$ increases rapidly within a few 0.1 K: it is 17(3) GHz at 2.1 K and ∼50 GHz above 2.2 K, where the dynamical line broadenings become too small to yield reliable values of the relaxation rate. The interaction most likely to be responsible for the Yb^{3+} fluctuations in this temperature range is the RKKY exchange interaction. In the magnetically ordered phase, the transverse fluctuations are less efficient for electronic relaxation because of the finite energy difference Δ_{ex} between the two states, whereas in the paramagnetic phase the two states are degenerate and relaxation is a zero-energy process,

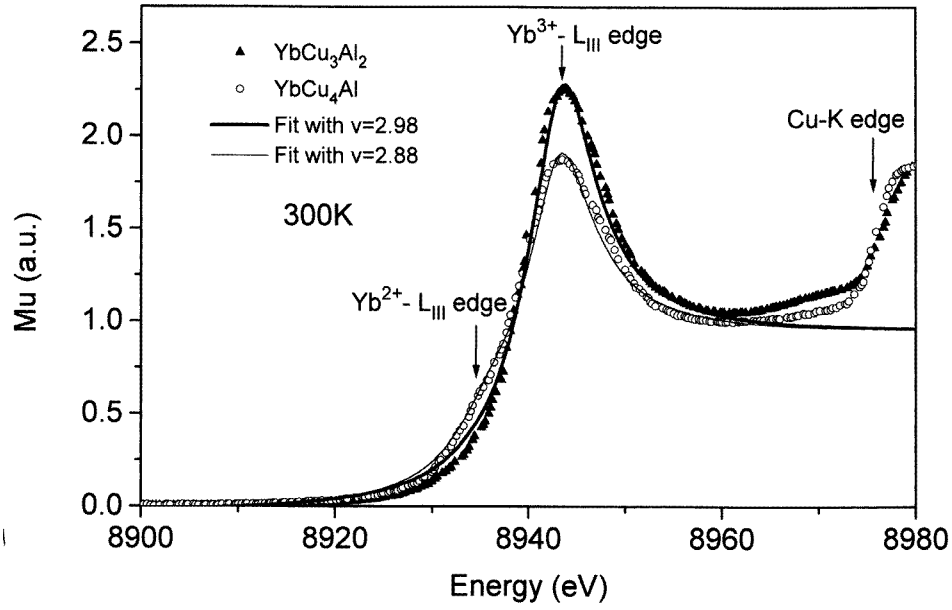

Figure 6. X-ray absorption (XANES) spectra near the Yb L_{III} edge at 300 K for the $YbCu_3Al_2$ sample and for $YbCu_4Al$. For $YbCu_4Al$, a sizeable Yb^{2+} component is visible. The lines are fits as explained in the text.

whence $1/T_1$ is larger. The rapid decrease of $1/T_1$ below 2.2 K is likely to be identified as the critical slowing down of the moment fluctuations as T approaches T_N.

8. The x-ray absorption (XANES) spectra at the L_{III} edge

The presence of a Mössbauer spectral component which shows a very weak thermal and field dependence raises the question of the presence of divalent, intermediate-valent or strongly Kondo trivalent Yb ions either in the $YbCu_3Al_2$ phase or in a separate impurity phase in our sample, besides the regular Yb^{3+} state. In order to check for this possibility, we performed x-ray absorption measurements close to the Yb L_{III} edge, at 10 K and 300 K, for our $YbCu_3Al_2$ sample, and also for an $YbCu_4Al$ sample. In $YbCu_3Al_2$, the spectra at the two temperatures are identical; the room temperature spectra of both compounds are represented in figure 6, the background being subtracted as described in reference [10].

The $YbCu_3Al_2$ spectrum (the black triangles in figure 6) shows mainly the peak associated with Yb in the trivalent state, at the Yb^{3+} L_{III}-edge energy $E_3 \simeq 8943$ eV. The $YbCu_4Al$ spectrum (the open circles in figure 6) also shows a dominant structure at the energy E_3, but a sizeable contribution is present at the Yb^{2+} L_{III}-edge energy $E_2 \simeq 8935$ eV. In order to estimate the valence of Yb from these spectra, we performed spectral simulations by superposing two arctangent functions, and two Lorentzian functions with peaks at energies E_3 and E_2. The relative weight of these two contributions defines the Yb valence v. The widths of the two arctangent functions, which correspond to the experimental resolution, have been taken as identical, as have the widths of the Lorentzian functions, which correspond to the Yb hole lifetime. From the fit of the $YbCu_3Al_2$ spectrum (the thick solid line in figure 6), we obtain a mean Yb valence $v = 2.98$, and we can estimate

that the upper limit for an Yb^{2+} contribution amounts to about 4%. From the fit of the $YbCu_4Al$ spectrum (the thin solid line in figure 6), we obtain a mean Yb valence $v = 2.88$. For both compounds, we notice that the width of the Lorentzian peak (4.5 eV) is somewhat larger than the width associated with the Yb hole lifetime (4 eV). This broadening can be related to stoichiometry defects or to a non-random distribution of Cu and Al on the 3g sites, as XANES is sensitive to the local environment of the Yb ion.

The XANES L_{III}-edge spectra in the $YbCu_3Al_2$ sample show therefore that it contains only trivalent (or almost trivalent) Yb, with a valency $v = 2.98(4)$. Then, the extra Mössbauer component can correspond either to an Yb-containing impurity phase where Yb is close to trivalent, or to almost trivalent Yb ions in the $YbCu_3Al_2$ phase, but with a local environment different from that of the majority Yb^{3+} ions. In both cases, these Yb ions must be more strongly hybridized than the majority Yb^{3+} ions because their Mössbauer spectrum is a field- and temperature-independent single line. Assuming that the extra component is an $YbCu_4Al$ impurity phase, with 25% relative weight, and assuming that Yb in $YbCu_3Al_2$ has a valence of 3, the mean Yb valence in our sample, as measured by XANES, would be 2.97, a value which lies within the error bar of the measurement.

9. Discussion and comparison with previous measurements

9.1. The Kondo coupling on the Yb^{3+} ion

The presence of a Kondo coupling on the Yb^{3+} ion in $YbCu_3Al_2$ has been inferred from the thermal variation of the magnetic resistivity, which shows negative ln T slopes, and from the specific heat jump at T_N, which is rather small ($\sim$4 J K^{-1} mol^{-1}) as compared with the expected value for a doublet ground state (12.4 J K^{-1} mol^{-1}) [2]. As magnetic ordering occurs below 2 K, the Kondo coupling is weaker than the RKKY exchange interaction [11]. In that case, the Kondo spin fluctuations must lead to a reduction of the spontaneous magnetic moment with respect to its CEF-derived value. Our analysis of the experimental data for $YbCu_3Al_2$ shows that the ground Yb^{3+} Kramers doublet is well described by an effective spin $S = 1/2$ with a g-tensor which, however, does not correspond to any of the hexagonal wavefunctions (6). The Yb^{3+} ground state cannot therefore be obtained with a model involving only the CEF interaction, and the wavefunction (7) cannot correspond to the ground state. We think that this discrepancy can be explained in terms of the Kondo coupling, in the following way: the effect of a weak Kondo coupling is to reduce the paramagnetic susceptibility for $T \leqslant T_K$, where T_K is the Kondo temperature, and hence to reduce the ground-doublet g-tensor components at low temperature. The ratio $g_\perp/g_z$, however, can be considered, in a first approximation, as reflecting the CEF-only value, if one assumes an isotropic reduction by hybridization. Then the true CEF ground wavefunction is such that $g_\perp/g_z \simeq 0.1$ and would be

$$|\psi_g\rangle = 0.99|\pm\tfrac{7}{2}\rangle \pm 0.14|\mp\tfrac{5}{2}\rangle. \tag{16}$$

It yields $g_z = 7.72$ and $\alpha_Q^{4f} = 5.7$ mm s^{-1}; the associated spontaneous moment along $\boldsymbol{c}$ is $m_{CEF}(0\ \mathrm{K}) = 3.85\ \mu_B$. The Kondo coupling in $YbCu_3Al_2$ would therefore reduce the spontaneous moment by 25%, leading to the measured value 2.85 μ_B. The saturation powder magnetization at 1.5 K would also be reduced from 2 μ_B/Yb^{3+} to the experimental value 1.5 μ_B/Yb^{3+}.

The Kondo temperature T_K can be obtained from the spontaneous-moment reduction at $T = 0$ K through the following approximate formula, derived from the variational solution

of the Kondo problem for a doublet ($N_f = 2$) [11, 12, 13]:

$$\frac{m(0\ \mathrm{K})}{m_{CEF}(0\ \mathrm{K})} = \sqrt{1 - \left(\frac{T_K}{T_{ex}}\right)^2} \tag{17}$$

where $k_B T_{ex}$ is the exchange energy, estimated from $k_B T_{ex} = |\lambda_c| m^2_{CEF}(0\ \mathrm{K}) \simeq 3.5$ K. One gets $T_K \simeq 2.3$ K, close to the estimate given in [2] based on the specific heat jump reduction at T_N ($T_K = 2.6$ K). The exchange energy scale T_{ex} is larger than the effective ordering temperature T_N, which is expected for Kondo lattices due to the competition between the Kondo spin fluctuations and the RKKY interaction in the establishment of long-range magnetic ordering [11]. For a doublet ground state, it has been shown via a self-consistent NCA calculation [14] that the Kondo magnetically ordered phase is well described by a mean-field theory. This is illustrated for the present $YbCu_3Al_2$ Kondo lattice by the fact that the thermal variation of the spontaneous Yb^{3+} moment follows a mean-field $S = 1/2$ law, and that the low-temperature properties are well described by an effective g-tensor, reduced by the Kondo coupling with respect to the pure CEF values.

9.2. The impurity phase

In order to understand the origin of the extra spectral component, we obtained Mössbauer spectra at 0.1 K and 4.2 K for different $YbCu_3Al_2$ samples. We found that the relative content of this component is sample dependent: in the present sample, which was also used for the magnetic measurements reported in [2], it amounts to ∼25%; in the sample used for the neutron diffraction experiments [4], it amounts to ∼15%, and for another sample submitted to microprobe analysis, which showed the presence of the $YbCu_3Al_2$ phase alone, an upper limit of 5% could be established. We think therefore that the extra spectral component corresponds to an Yb-containing impurity phase in which, according to the L_{III}-edge spectra, the Yb ion is almost trivalent. In all of these samples, the Mössbauer spectra of the main $YbCu_3Al_2$ phase show no significant difference at 0.1 K and 4.2 K. The presence of this impurity phase therefore does not modify the magnetic properties of the $YbCu_3Al_2$ phase, but it illustrates the difficulty of Yb alloy metallurgy, due to the high vapour pressure of this element, especially when large amounts of alloy are prepared.

The identification of the impurity phase relies on the fact that it cannot be detected in the x-ray or neutron diffractograms, and therefore it must be one of the $YbCu_{3+x}Al_{2-x}$ phases, for $0 < x \leqslant 1$, whose lattice parameters are very close to those of $YbCu_3Al_2$. A preliminary ^{170}Yb Mössbauer study of $YbCu_4Al$ provides a strong hint that this compound is the impurity phase in our samples. The spectrum of $YbCu_4Al$ consists of a slightly asymmetrical single line, very similar to the extra spectral component in the $YbCu_3Al_2$ sample, and showing also a very weak thermal dependence. This can be understood because previous measurements [2] have shown that $YbCu_4Al$ is a Kondo lattice with a large Kondo temperature, as evident from its very large paramagnetic Curie temperature $\Theta_p \simeq -340$ K. The presence of ∼25% of $YbCu_4Al$ in the $YbCu_3Al_2$ sample used for magnetic measurements [4] also accounts for the rather low derived effective moment of 4.14 μ_B/Yb (the free-ion value is 4.54 μ_B). As regards the magnetization curve (figure 5), the presence of $YbCu_4Al$ has no influence due to the very low susceptibility of the latter (0.15 μ_B/Yb at 7 T [2]).

9.3. Comparison with the neutron diffraction data

According to the neutron diffraction study of $YbCu_3Al_2$ [4], the magnetic structure is of antiferromagnetic type, with magnetic moments parallel to the crystal $\boldsymbol{c}$-axis. Their saturated

value, according to the structural model derived in [4], is 2.1 μ_B. The transition temperature deduced from the thermal variation of the magnetic Bragg peaks is 1.6 K.

The ^{170}Yb Mössbauer data agree with the neutron data as to the direction of the spontaneous moment and its order of magnitude, but they are at odds with the neutron results concerning the exact moment value, which is found to be larger (2.85 μ_B) than the neutron result, and the transition temperature, which is also found to be higher (2 K) than the neutron result. These are rather serious discrepancies, for which we have at present no real explanation. The neutron-derived spontaneous-moment value is somewhat underestimated due to the 15% content in non-magnetic $YbCu_4Al$; the corrected value is 2.3 μ_B, which is still lower than the Mössbauer-derived value. In metallic compounds, the hyperfine field at the ^{170}Yb nucleus can contain a contribution coming from conduction band polarization, which can be of the order of magnitude of a few 10 T [15]. The neutron diffraction technique would also detect this polarization as a small extra magnetic moment at the Yb site. The discrepancy between the Mössbauer- and neutron-derived moment values could be explained if the conduction band polarization led to a *positive* contribution to the hyperfine field and to a *negative* contribution to the magnetic moment. The latter is obtained in the presence of the Kondo effect, if one considers spin-only polarization (s-type conduction electrons) and if one remains within the frame of the simple $J_K \boldsymbol{s} \cdot \boldsymbol{S}$ model, with $J_K < 0$. In this case, indeed, the ratio of the conduction and 4f polarizations is proportional to J_K, i.e. it is negative. However, the presence of various mechanisms for the hyperfine coupling and of orbital contributions to the conduction electron polarization renders the evaluation of the hyperfine contribution difficult, and one can only retain the above-described mechanism as a possible explanation for the difference between Mössbauer-derived and neutron-derived moment values.

10. Conclusion

The magnetic and crystal-field properties of the Yb^{3+} ion in the hexagonal alloy $YbCu_3Al_2$ have been investigated by ^{170}Yb Mössbauer spectroscopy and L_{III}-edge x-ray absorption spectroscopy, for a polycrystalline sample. In the antiferromagnetic phase, we find that the Yb^{3+} spontaneous moment lies parallel to the crystal $\boldsymbol{c}$-axis, in agreement with previous neutron diffraction results, and that its saturated value is 2.85 μ_B, whereas the (corrected) neutron-derived value is 2.3 μ_B. The thermal variation of the spontaneous moment has been obtained through the measurement of the hyperfine field between 0.1 K and 1.5 K; between 1.5 K and 2 K, the Mössbauer lineshapes are influenced by electronic fluctuations, and the spontaneous moment has been obtained via a relaxational lineshape where the parameters are the exchange splitting and the relaxation frequency $1/T_1$. The magnetic transition is found to be of second order, with $T_N = 1.95$ K, the measured molecular-field constant is $\lambda = -0.35\ T/\mu_B$ and $1/T_1$ is $\simeq$5 GHz, corresponding to fluctuations induced by the transverse part of the RKKY exchange interaction. In the paramagnetic phase, a spectrum at 4.2 K with an applied magnetic field of 4 T yielded the ground-doublet g-tensor components: $g_z = 5.7$, in agreement with the saturated spontaneous-moment value; and $g_\perp/g_z \simeq 0.1$, which allows the magnetization curve at $T = 1.5$ K to be correctly reproduced. These g-tensor components however do not correspond to any of the hexagonal crystal-field wavefunctions; we interpret this fact in terms of the Kondo effect on the Yb^{3+} ion, with a Kondo temperature $T_K = 2.3$ K close to that derived from the reduction of the specific heat jump at the magnetic transition. The bare crystal-field ground wavefunction appears then to be an almost pure $|J = 7/2; J_z = \pm 7/2\rangle$ doublet. The thermal variation of the 4f-shell quadrupolar moment indicates that the first excited crystal-field state is an

almost pure $|J = 7/2; J_z = \pm 5/2\rangle$ doublet, with an energy $\Delta \simeq 100$ K. Finally, the L_{III}-edge x-ray absorption spectra at 10 K and 300 K do not detect any contribution from an Yb^{2+} configuration, which agrees with the picture of an Yb ion very close to trivalent with a weak Kondo coupling.

Acknowledgments

We thank E Alleno and C Godart, from CNRS-Meudon (France) and LURE-Université d'Orsay (France), for performing the L_{III}-edge x-ray absorption measurements.

References

[1] For a review, see
Brandt N B and Moshchal'kov V V 1984 *Adv. Phys.* **33** 373
[2] Bauer E, Hauser R, Gratz E, Gignoux D, Schmitt D and Sereni J 1992 *J. Phys.: Condens. Matter* **4** 7829
[3] Bauer E, Payer K, Hauser R, Gratz E, Gignoux D, Schmitt D, Pillmayer N and Schandy G 1992 *J. Magn. Magn. Mater.* **104–107** 651
[4] Bauer E, Gratz E, Keller L, Fischer P and Furrer A 1993 *Physica* B **186–188** 608
[5] Alleno E, Hossain Z, Godart C, Nagarajan R and Gupta L C 1995 *Phys. Rev.* B **52** 7428
[6] Bonville P, Hodges J A, Imbert P, Jaccard D, Sierro J, Besnus M J and Meyer A 1990 *Physica* B **163** 347
[7] Abragam A and Bleaney B 1969 *Electron Paramagnetic Resonance of Transition Ions* (Oxford: Clarendon)
[8] Bonville P, Canaud B, Hammann J, Hodges J A, Imbert P, Jéhanno G, Severing A and Fisk Z 1992 *J. Physique* I **2** 459
[9] Gonzalez-Jimenez F, Imbert P and Hartmann-Boutron F 1974 *Phys. Rev.* B **9** 95
[10] Rohler J 1985 *J. Magn. Magn. Mater.* **47+48** 175
[11] Doniach S 1977 *Physica* B **91** 231
[12] Yamamoto T and Ohkawa F J 1988 *J. Phys. Soc. Japan* **57** 3562
[13] LeBras G 1994 *Thesis* Orsay–Paris XI University
[14] Bonville P, Polatsek G, Hodges J A, Imbert P and LeBras G 1993 *Physica* B **186–188** 254
[15] Berthier Y, Devine R A B and Belorizky E 1978 *Phys. Rev.* B **17** 4137